

# Validating the MISR radiometric scale for the ocean aerosol science communities

Carol J. Bruegge, Wedad Abdou, David J. Diner, Barbara J. Gaitley, Mark Helmlinger, Ralph A. Kahn, & John V. Martonchik

*Jet Propulsion Laboratory, California Institute of Technology, Pasadena, California*

**ABSTRACT:** The Multi-angle Imaging SpectroRadiometer (MISR) is one of five instruments on-board the EOS/ Terra spacecraft. Nine cameras, which view up to 70° forward and aft of the spacecraft track and enable unique geophysical retrievals, provide this multi-angle capability. As an example, many on-orbit sensors are able to estimate the amount of aerosol loading present in the underlying atmosphere. MISR, however, is capable of retrieving information on both aerosol amount and microphysical properties. A necessary prerequisite, however, is that the instrument be calibrated to its absolute, band, and camera-relative specifications. Previous work has demonstrated that MISR is calibrated to better than 4% absolute uncertainty (1 $\sigma$  confidence level) for bright land targets. This paper validates that radiometric accuracy is maintained throughout the dynamic range of the instrument. As part of this study, a new look has been taken at the band-relative scale, and a decrease in the radiance reported for the Red and NIR Bands has resulted. The calibration processes is now routine, fully developed, and tested. Bi-monthly on-orbit calibrations will be continued throughout the life of the mission and allow MISR to accurately report incident radiances, even in the presence of expected sensor response changes.

## 1 INTRODUCTION

### 1.1 *Science drivers to accurate radiometry*

The Multi-angle Imaging SpectroRadiometer (MISR) (Diner et al. 1998b & 2002) is one of five instruments on-board NASA's Earth Observing System (EOS). Data products include cloud height and albedos, surface bi-directional reflectances, and aerosol parameters. (Aerosols are airborne particles derived primarily from urban and industrial pollution, forest fires, volcanoes, sea spray, and desert dust.) These measurements are routinely provided over the globe, and are important in understanding Earth's radiation budget and climate change.

One unique contribution that can be made by MISR is providing aerosol products with improved accuracies and with some degree of distinguishability. Calibration accuracy is particularly important for aerosol retrievals over dark ocean targets. Based upon theoretical studies, Kahn et al. (1998 & 2001) provide a clear statement of the MISR prelaunch aerosol science objective for such conditions. "We expect to retrieve column optical depth from measurements over calm ocean for all but the darkest par-

ticles, with typical size distributions and compositions, to an uncertainty of at most 0.05 or 20%, which ever is larger, even if the particle properties are poorly known. The measurements should also allow us to distinguish spherical from nonspherical particles, to separate two to four compositional groups based on indices of refraction, and to identify three to four distinct size groups between 0.1 and 2.0  $\mu\text{m}$  characteristic radius at most latitudes." To achieve this goal in practice requires accurate top-of-atmosphere (TOA) radiances. The validation of MISR radiometry under low-light conditions is not only of interest to the ocean aerosol science community, but also to the dense, dark vegetation, and ocean surface color communities.

Top-of-atmosphere equivalent reflectance is defined here as  $\rho_{\text{toa}} = (\pi L/E_0)$ , where  $L$  is the TOA radiance within a given MISR band, and  $E_0$  is the MISR total-band-weighted exo-atmosphere solar irradiance, derived from the World Climate Research Program (WCRP, 1986) published values of solar irradiance. Very low light levels, in the equivalent reflectance range below 7%, are typically found over dark water scenes having aerosol burdens on the order 0.2 or less at mid-visible wavelengths. Here the desired MISR radiometric calibration accuracy is at the cutting edge of current capabilities. The needed constraint amounts to  $\Delta\rho_{\text{toa}} = 0.002$  or better, for

equivalent reflectance below 0.02, in all channels. This translates to a 10% absolute uncertainty at a scene equivalent reflectance of 0.02.

MISR calibration requirements for bright targets ( $\rho_{eq}=1$ ) include 3% absolute, and 1% band and camera-relative calibrations. MISR radiometric accuracy has previously been documented (Bruegge et al. 2002) for homogeneous desert targets. Here vicarious calibration (VC) experiments, in conjunction with sensor cross-comparison studies and on-board-calibrator (OBC) error assessments, have demonstrated that MISR radiances are uncertain to within 4% ( $1\sigma$ ) - for targets which fall mid-range in the sensor's dynamic range ( $\rho_{toa}=0.3$  to 0.4). Vicarious calibration experiments are intensive field campaigns, located at uniform desert sites such as Railroad Valley, Nevada. These are conducted annually for MISR, by the Jet Propulsion Laboratory (JPL) staff (Abdou et al. 2002). Unique tools for this JPL operation include AirMISR (Diner et al. 1998a), an ER-2 based aircraft prototype for MISR, and the PARABOLA instrument (Bruegge et al. 2000, Abdou et al. 2000), a surface based radiometer that measures upwelling and downwelling radiance in  $5^\circ$  samplings. For these desert VC experiments the surface reflectance term dominates the TOA radiance. Under clear sky and low aerosol conditions, typical for southwestern sites, radiances are measured within an uncertainty of 3%. Vicarious calibrations are used to validate the radiometric scale of some sensors. In the case of MISR, the June 2000 vicarious campaign was used to calibrate the on-board-calibrator, which in turn produces radiometric gain coefficients for the cameras on a bi-monthly basis.

Validation of MISR radiometry over desert targets does not necessarily assure accuracy over dark ocean sites. Instrument artifacts, such as additive stray-light or electronic biases, if present, would lead to large radiometric errors in the measure of incident radiance. These could be as large or larger than the actual radiance to be measured. Although dark water vicarious calibrations can be conducted, they are not routine. For these cases the atmospheric contribution to top-of-atmosphere radiance dominates the surface term, and the process of computing top-of-atmosphere radiances from in-situ measurements is less certain. Cross-comparisons with other sensors provide an alternate validation approach. The Terra/MODerate-resolution Imaging Spectroradiometer (MODIS) instrument is one possible cross-comparison source. Co-located on the same platform, MODIS and MISR view a scene simultaneous in time and with similar bandpasses. Unfortunately ocean images acquired by nadir-viewing sensors, such as MODIS, are frequently contaminated with ocean glint. The large radiance gradient of these scenes makes data comparisons less reliable.

The validation of MISR radiometry over dark targets has proceeded with all proposed approaches: 1)

an error-tree analysis of the potential contributors to low-light errors, 2) cross-comparisons with MODIS scenes, 3) use of a lunar calibration experiment, and 4) dark water vicarious calibrations. The first three of these topics are covered in this publication.

A dark-water vicarious calibration of MISR has been described by Kahn et al. (2004). Here data from the AERosol ROBotic NETwork (AERONET), in conjunction with an ocean reflectance model and radiative transfer calculation are used to predict top-of-atmosphere radiances, which are then compared to MISR and MODIS. AERONET-based radiances are found to be systematically lower than MISR, by about 10%. MISR and MODIS ocean channels are found to agree within 4%, with MISR reporting higher radiances. The agreement of MISR with MODIS ocean channel data, over ocean sites, is consistent with the agreement with MISR and MODIS land channel data, over land sites. These data indicate that MISR ocean data are valid to within the needed uncertainty, for these nadir observations.

The validation of MISR radiometry over very bright targets, such as clouds, has been reported elsewhere (Marchand, 2004). Cloud studies have demonstrated that MISR radiance data over very bright targets are consistent with simulations and cross-sensor comparisons, again to within 4% uncertainty.

## 1.2 *The MISR instrument*

MISR produces global data sets at nine-day intervals or less, depending on latitude. The effective center wavelengths, given in Table 1, have been computed using a moments (centroid) analysis within the region delimited by the 1% response points (Bruegge et al. 2002). The effective bandwidths are also given. These parameters are used to define an equivalent square-band response function and to summarize instrument characteristics. Band weighted (both in-band and total-band) exo-atmospheric irradiance values are also shown. As Level 1B radiances have not been adjusted to remove out-of-band response, total-bandpass solar irradiance values are used to compute Level 1B equivalent reflectances. Approximately 3% of the camera output come from signals at wavelengths outside the 1% limits, for a spectrally neutral scene.

Each of the nine cameras has a unique name, and is associated with a specific view angle. The cameras view a target consecutively in the order Df ( $70.5^\circ$  fore), Cf ( $60.0^\circ$ ), Bf ( $45.6^\circ$ ), Af ( $26.1^\circ$ ), An (nadir), Aa ( $26.1^\circ$  aft), Ba ( $45.6^\circ$ ), Ca ( $60.0^\circ$ ), and Da ( $70.5^\circ$ ), with 7 minutes from first to last acquisition of a target. Here the first letter of the camera name refers to the lens design and the second designates the fore-, nadir-, or aft-view directions with respect to the spacecraft track. MISR has 14-bit quantization, and therefore has roughly 16,384 gray levels

(the finite video offset and square-root encoding reduces this by about 300 counts). A signal of  $\rho_{\text{toa}}=0.02$  results in an output DN of from 300 to 800 DN, depending on the detector. For dark targets, errors of 30 DN may begin to affect radiometric accuracy significantly.

Table 1. MISR spectral parameters

$\lambda_c$ in-band	$\delta\lambda$ in-band	$E_{0,b}$ in-band	$E_{0,b}$ total-band
nm	nm	$\text{W m}^{-2} \mu\text{m}^{-1}$	$\text{W m}^{-2} \mu\text{m}^{-1}$
447	41	1871	1867
558	27	1851	1842
672	20	1525	1524
867	38	969.6	977.8

MISR cameras acquire data in a pushbroom configuration, using the spacecraft motion to build up an image from each of the 36 charge-coupled device (CCD) linear arrays. The spatial resolution of the MISR cameras, established by the size of the detector elements, optical focal length, and spacecraft altitude, is 275 m crosstrack (for the off-nadir cameras), or 250 m (for the nadir viewing camera). Downtrack instantaneous field-of-view increases due to view angle effects, ranging from 214 m in the nadir to 707 m at the most oblique angle. Downtrack sampling is 275 m for all cameras. In practice, most data are acquired in Global Mode, where pixel averaging is performed in order to reduce the data rate. Here 24 of the 36 data channels have been 4x4 sample averaged before transmission from the instrument. For these channels data are transmitted at 1.1 km resolution. Even in Global Mode, however, high-resolution pixels are maintained for the four nadir channels, and the eight additional Band 3/ Red channels. Complete high-resolution data sets for all 36 channels can be obtained from an instrument configuration called Local Mode. Here specific sites are targeted, such as those where intensive field campaigns are being conducted. The size of a Local Mode region is 300 km downtrack by 380 km crosstrack. About a dozen Local Mode sites are acquired routinely, including observations over desert calibration sites.

The sections to follow discuss the operational calibration processes, error analysis of the radiometric products for low light conditions, and the validation studies applicable to these low-light conditions.

## 2 THE CALIBRATION PROCESS

### 2.1 On-board calibrator

Radiometric data products include geo-located radiance images at nadir and off-nadir Earth view angles. These are total band-weighted camera-incident radiances, in units of  $\text{W m}^{-2} \text{sr}^{-1} \mu\text{m}^{-1}$ . The MISR radiometric response scale is established by use of an on-board calibrator (OBC), as well as vicarious calibration experiments (Bruegge et al. 1993a). The strength of the OBC is its ability to provide camera, band, and pixel-relative calibrations, as well as to measure temporal stability. Experiments using the OBC are conducted once every two months. The bi-monthly frequency is desirable in that it is prudent to deploy the calibration panels only as needed to capture camera response changes. (The MISR cameras have degraded by no more than 2% per year, as reported by Bruegge et al. 2002.) The OBC consists of two Spectralon diffuse panels, and six sets of photodiode detectors. The latter measure solar-reflected light from the panels, and provide a measure of the camera-incident radiance. These are regressed against the camera output, in order to provide the radiometric response for each of the 1504 CCD detector elements per line array, nine cameras, and four spectral bands per camera. One such photodiode set is on a goniometric arm, and allows panel bi-directional reflectance factor (BRF) degradation to be monitored. Photodiodes are either of a light-trapped design called High Quantum Efficiency (HQE) diodes, or PIN photodiodes. The latter are constructed with a single diode per package.

Although OBC system degradation can occur in principle, MISR experiment accuracy has benefited from the stability of the calibrator with time. Prelaunch testing (Bruegge et al. 1993b, Stiegman et al. 1993) established Spectralon preparation and handling procedures that would reduce the risk of on-orbit degradation. Hydrocarbon contaminants introduced during manufacture or testing, such that due to machining oils, were shown to cause degradation when exposed to on-orbit vacuum ultraviolet light. With this information at hand the MISR Spectralon panels were vacuum baked, following laboratory reflectance testing, to remove any such contaminants. In addition, the project elected to swap out the panels present during instrument integration and spacecraft-level testing. Prior to launch the original panels were removed and replaced with panels that had been kept in a nitrogen-purged container, following vacuum baking. Degradation analysis on the on-board calibrator (Chrien et al. 2002) has demonstrated the success of this plan. The flight Spectralon panels have degraded, on-orbit, by no more than a total of 0.5%.

Degradation of the Spectralon panels would be of concern if the BRF were to change in shape, or if the relative spectral reflectance were to change, at MISR wavelengths. Since MISR makes use of in-flight detector standards, a decrease in the panel's hemispheric reflectance would otherwise be inconsequential. The blue-filtered High Quantum Efficient (HQE) device, a light-trapped three detector radiometer, has remained stable to better than 0.5% throughout the mission (Chrien et al. 2002). This diode is therefore used as the primary standard. Not all of the monitoring photodiodes have remained stable on-orbit. For this reason, all other photodiodes are recalibrated against this standard prior to the bi-monthly data analysis.

The reduction of the OBC experiment data begins with an assumption that the instrument response can be modeled as:

$$DN - DN_0 = G_1 L_b \quad (1)$$

where:

- $L_b$  is the incident spectral radiance, weighted over the total-band response function,
- DN is the camera output digital number,
- $DN_0$  is the DN offset, unique for each line of data, as determined by an average over the first eight "overclock" pixel elements (output samples which follow clocking of the CCD line array), and
- $G_1$  are linear gain coefficients that provide the radiometric calibration of a specific pixel.

Originally it was believed that the photodiodes could be used to measure panel-reflected light as the Sun-panel path traversed a varying amount of the Earth's atmosphere. This would provide radiance and DN points along the sensors response curve, including low-light levels, and hence determine camera linearity and offset. Several lines of evidence lead us to conclude that we should not utilize atmospherically attenuated data. These are:

- Photodiode linearity. The linearity of the photodiodes cannot be validated at  $\rho_{toa}$  less than 0.03. Levels below this are outside the linearity range of the preamplifiers.
- Photodiode offset. A finite photodiode output offset is known to exist, but is not well characterized, due to digitization error for these units. Offset knowledge would be required for low-light measurements, but can be ignored at higher light levels.
- Refraction. Much of the signal observed at the low-light levels has been deviated by refraction, as light traverses the Earth's atmosphere. The signal is attenuated differently with time, depending on spectral band.
- BRF uncertainties. There is increased uncertainty in the laboratory measured Spectralon BRF database for large illumination and view angles, as are encountered at low-light levels. For these cases Spectralon becomes more non-lambertian and the BRF in-

creases. Extrapolations to geometries outside the limits of the measured BRF database are highly uncertain.

These issues have led the MISR team to reject any calibration data that has been contaminated by the Earth's atmosphere, and to adopt a linear calibration equation rather than a more complex form. The linear method is often referred to as a two-point calibration, since only the gain and offset need be determined. The gain is computed from DN and radiance pairs measured when the Sun-spacecraft path is free of the Earth's atmosphere. The offset term is set equal to the system electronic bias. As the dark current is too small to measure, the DN value assumed for a zero incident radiance is equal to the system electronic bias, as measured by  $DN_0$ .

The results of these and other OBC validation studies (Chrien et al. 2002) have led us to use the OBC as a stability monitor, with the absolute scale determined by vicarious calibration experiments.

## 2.2 Process updates

MISR radiometric coefficients are delivered in a file named the Ancillary Radiometric Product (ARP). Over time the processing algorithm used to derive these coefficients has changed. Table 2 summarizes these revisions. Each change has incrementally reduced radiometric uncertainty. From this table we see that a band adjustment was made to MISR radiances, for data processed after November 2003. The analysis that led to this adjustment is given in Section 2.4, and is based upon studies of data processed with the previous (linear-offaxis) algorithm.

Table 2. ARP algorithm revision history. ARP files are designated by a format Tx\_y, where x are the experiment indices (time), and y is the revision number for a given Tx file. T=1 represents preflight-computed coefficients.

### HQE-Blue.

- The blue-filtered HQE photodiode is used as the primary radiometric standard. This device is selected based upon its stability with time.

Impact: First calibration attempt. Uses preflight calibration of the Blue HQE diode - on-orbit validation not yet in place.

Date: T2\_4: Aug. 24, 2000

### VC scaling.

- The June 11, 2000 vicarious calibration experiment is used to calibrate the HQE-Blue photodiode standard.

Impact: 9% increase in MISR radiometric scale.

Date: T2\_5: Feb. 24, 2001

### Quadratic.

- A quadratic calibration equation is introduced, believed to show an improvement in the radiances reported over dark targets, such as oceans.

Impact: Changes in MISR reported radiances are negligible for equivalent reflectances >0.02, and a few percent otherwise.

Date: T8\_1: May 17, 2001

Provisional.

- The South Pole calibration panel is shown to have measured bi-directional reflectance function (BRF) data that agree with the preflight determination. The goniometer is used to update the BRF profile for the North calibration panel.

Impact: Aft-camera radiances decreased by a few percent.

Date: T12\_1: Dec. 22, 2001

Linear-offaxis (Linear equation & off-axis correction).

- A linear calibration is restored.

- Data ignored that are contaminated by the Earth's atmosphere.

- Fixes error in BRF indexing code which caused an error for radiance reported an off-axis view angles.

Impact: - Linear equation is less risky.

- Eliminating data contaminated by the Earth's atmosphere increases experiment accuracy.

- Error fix does not impact on-axis radiances.. Greatest improvement is for An-camera west edge of swath (10% change).

Date: T17\_1: Oct. 24, 2002

Band-adjust.

- Decreases Red band radiance by 3% and NIR by 1%

Impact: Radiances are more consistent with vicarious

Date: T24\_1: Dec. 5, 2003

In order to understand data heritage, MISR data users should document the version number of the products they use. For Level 1B products, they should document the ARP version used to generate their data. To determine which ARP file was used to produce a Level 1B data product, one would use an HDF browser, such as hdfscan. (This software is available from the Langley DAAC, <http://eosweb.larc.nasa.gov>, and was written to view MISR data as well as generic HDF files). Using such a data browser, one can read the metadata published within the MISR data product. The ARP file name can be found under Annotation Text: Input Data files. This file name can be compared to the latest delivered ARP file name, for a specific time period.

### 2.3 Vicarious calibration

The MISR team has conducted annual vicarious field campaigns, using desert targets in the southwestern United States. As MISR radiances change with processing algorithm updates, the ratio of MISR to VC radiances may also change. In order to look for consistent biases with respect to MISR, a comparison must be made with a common processing algorithm. This was done using the "linear-offset" algorithm (see Table 2), which was in place through October 2003. The results are shown in Figure 1.



Figure 1. An-camera vicarious calibration results for nadir Terra overpass dates. Lines from top to bottom are: square) 30-June-2001, Railroad Valley; circle) 07-July-2003, Black Rock Desert; dash) 22-July-2003, Railroad Valley; dash) mean; diamond) 06-Jun-2000, Lunar Lake; triangle) 10-Jun-2002: Ivanpah playa. All playa are located in Nevada.

For these experiments data were acquired at Lunar Lake, Railroad Valley, Ivanpah, and Black Rock Desert (all located in Nevada). Of these, Ivanpah is the smallest playa, roughly 2 km across. Although MISR Level 1B data are corrected for point-spread-function response, as part of the standard processing, the data are exceptionally low, indicating that some residual out-of-field effect may still be present at the 1% level. Excluding Ivanpah, the precision of the vicarious calibration process appears to be 2-4% and smallest for the Green and Red spectral bands. The dashed line in Figure 1 shows the mean of these calibrations. These multi-year data do not show any systematic change in the reported MISR calibration, to within the precision of the vicarious calibration methodology. For this reason, no updates have been made to the response coefficient of the OBC primary photodiode standard (Blue-HQE), other than its initial adjustment in February 2001.

### 2.4 Band-relative adjustment

For these "linear-offset" data, the band-relative scale was determined as follows:

1) The June 2000 VC campaign was used to calibrate the Blue-HQE photodiode, the OBC primary standard. (This transfer establishes the 2000 VC campaign as the absolute radiometric standard for the MISR experiment.) If needed, future VC experiments could be used to update the response of this primary standard, as may be needed if photodiode degradation is measured.

2) For each bi-monthly experiment the measured radiance from the Blue-HQE photodiode is used to predict the band-weighted radiances for the secondary photodiodes. Differences in field-of-view are taken into account, and the Spectralon reflectance is assumed to be spectrally invariant (Bruegge et al. 2001). The latter assumption is uncertain at the 1% level, but impacts our experiment to a lesser degree. For example, Early et al. (2000) published results of a Spectralon BRF-measurement round robin that involved several institutions, including JPL and the

National Institute of Standards and Technology (NIST). From this study we see that reflectance of Spectralon, in our Red band, is 0.1% larger than that for the Green band. (MISR BRF data were acquired at the HeNe laser wavelength of 632 nm.) This result is for a solar illumination angle of 45° and for the nadir viewing pixels, which have the largest viewing angles to the panel. Although the Early report does suggest there is some wavelength dependence to the Spectralon's reflectance, we do not believe it is sufficient to explain the wavelength-dependent biases shown in Figure 1.

3) The response coefficient of each secondary diode is adjusted such that the measured and Blue-HQE derived radiances agree. This step removes any response degradation from the secondary photodiodes. (The photodiodes have degraded differently for the different wavelengths. As an example, the Green and NIR HQE response has changed by 5% and 10%, respectively.)

4) The secondary photodiodes are used to calibrate the cameras, with filter-matched diode and camera pairs used in turn. The nadir-viewing PIN is used to calibrate the An camera and Da and Df off-nadir PINs are used to calibrate the eight off-nadir cameras. BRF corrections is required for the C, B, Aa and Af cameras, as there are no photodiodes at these angles.

With this "linear-offaxis" process in place, we see from Figure 1 that there is an inconsistency with wavelength, in comparing VC radiances to MISR-measured radiances. In particular, looking at the mean VC comparison, we see that the MISR radiances are about 3% too high in the Red, and 1% too high in the NIR.

Figure 2 shows this same mean VC result, but in addition plots the MISR-lunar comparison, to be discussed in Section 4.2. For this band-relative comparison, a 5% bias was removed at all wavelengths from the lunar curve. The consistency of these VC and lunar band-relative results demonstrates the consistency of our band-dependent biases. It is noted that these two studies cover a range of target radiances and scene contrasts. The desert targets are roughly 0.3 in equivalent reflectance, the lunar surface approximately 0.04; the desert target is homogeneous and extensive, whereas the lunar target covers only a fraction of the MISR field-of-view.

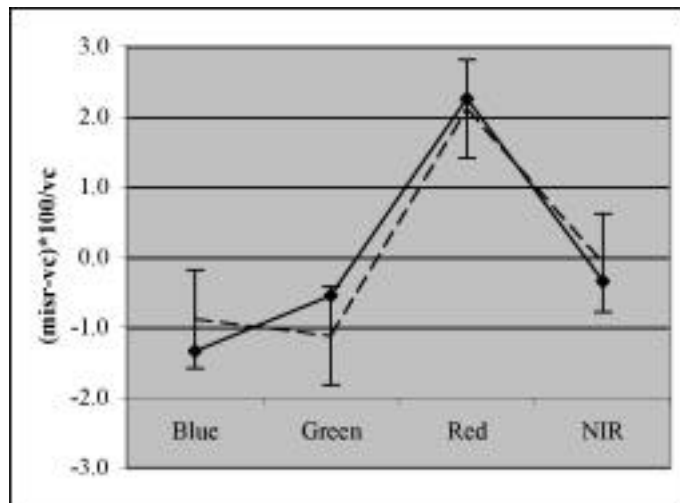


Figure 2. Comparison of mean vicarious calibration (dashed line) results with bias-removed Lunar data (solid line).

Based on these results, supported by Kahn et al. (2004), MISR radiance data products processed after November 2003 have a 3% decrease in the red band and 1% in the NIR. The correction compensates for a systematic error whose origin remains unknown at this time.

### 3 ERROR SOURCES

The fabrication of a precision camera, such as MISR, begins with the design of a stable sensor, continues with a component characterization, and is followed with a system-level evaluation. These steps provide: 1) a lower-bound on the experiment uncertainty, 2) a sufficient knowledge of the system such that deviations from the performance specifications, if detected, can be proposed and implemented, and 3) allow design lessons-learned to be documented for the benefit of future missions. As part of this routine system analysis, potential contributors to radiometric uncertainty, specifically at low-light levels, have been investigated. These error-sources are discussed in the following sections.

#### 3.1 Electronic offset: Baseline stabilization

MISR camera signal chains incorporate a circuitry called BaseLine Stabilization (BLS). The BLS circuitry was incorporated into the MISR design in order to adjust for sudden changes in the system response, as could follow radiation-induced damage to the detector, or in the event of undesirable operational amplifier feedback. The circuitry adds a floating electronic pedestal to the signal chain. In the presence of a sudden change in the incident illumination, the BLS stabilizes its output in about 75 lines (3 seconds). In order to measure the light-induced portion of the signal, this offset must be subtracted. We estimate this offset by use of overclock pixels.

MISR detectors clock out 512 samples of the serial register. These follow reading of the light-sensitive portion of the signal chain. Of these, eight are transmitted from orbit with the active-pixel data. The average of these eight overclock pixels is computed, and used as a measure of the electronic offset,  $DN_o$ . The BLS circuitry also makes use of these overclock pixels to drive the signal chain electronics to -2.9 V, when no optical illumination is present. It is not known whether the BLS circuitry samples the same samples that are transmitted to the ground.

There are several uncertainties associated with usage of the BLS circuitry:

- Preflight testing has shown that the 512 overclock pixels are not constant for a given line of data. Further, we do not know which of the 8 overclock samples are used to establish the BLS output which controls the magnitude of the electronic offset. There is therefore some uncertainty, which can be quantified as the difference in the overclock over the 512 samples.

- In theory the BLS should be independent of illumination level. This is found not to be the case, presumably because of light leaking into the serial register even after the CCD signal has been clocked out. This deviation reduces our confidence in measuring the electronic offset. A light leak would cause  $DN_o$  to underestimate the bias signal to subtract.

- The effective offset signal could vary spatially across the active array, and thus no one value of  $DN_o$  would accurately represent the electronic bias. Light leakage into the serial array is one such mechanism by which a spatially variable bias signal could be induced across the CCD array.

With these potential errors we can bound the radiometric uncertainty due to BLS. If we are correctly using the first 8 overclock samples as a representation of the electronic pedestal, then there is no error in the static-illumination case. If the electronic pedestal is better represented by the last eight overclock samples, then the error is 20 counts out of 300 DN. This is a 7% error for a 2% equivalent reflectance signal (worst case error for a homogeneous scene). This BLS uncertainty error would be larger for mixed ocean/cloud or ocean/snow and ice scenes. Here the bright targets would drive up the overclock as well as contribute to leakage into the shield register.

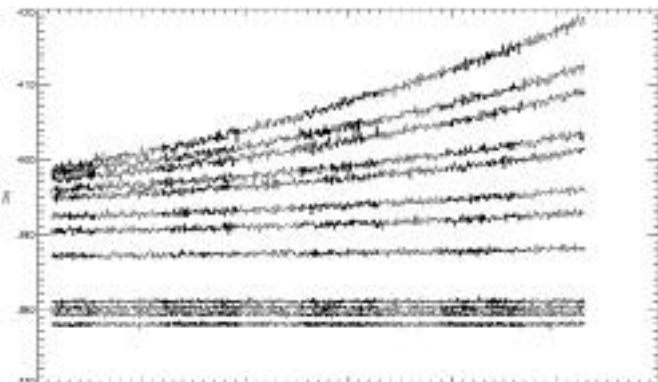


Figure 3. DN from the 512 extended overclock pixels as measured during preflight testing. Each line is the response to integrating sphere illumination, spanning the range of equivalent reflectance from 0.05 to 1.0.

### 3.2 Electronic offset: Dark current

Detector full well capacity is roughly 1 million electrons and data are digitized to 14 bits. Thus, we have about 60 electrons per DN bin. The CCD readout rate is 40 msec, and the pixel size is 21  $\mu$ m. The dark current can be expressed as:

$$D=2.5 \times 10^{15} P N T^{1.5} e^{-E_g/(2kT)} \quad (2)$$

where P is the pixel size ( $\text{cm}^2$ ), N is the dark current at 300 K, 26.85 C ( $\text{nA}/\text{cm}^2$ ),  $E_g$  is the silicon band-gap energy (eV), k the Boltzmann constant, and T the operating temperature (K). (This equation has been provided by Janesick, Thermal dark current tutorial, <http://www.pvinc.com/janesicks-therm-letter.htm>).

This equation shows that for our  $-5^\circ$  C operating temperature, the digitized dark current is 1 DN. It is noted that this is an overestimation, as charge is collected only over the integration time (roughly 20 msec), and that the actual pixel area is  $21 \times 18 \mu\text{m}$ .

In reviewing MISR's measured dark current, we have observed a digitized dark current of 0 or 1 DN, for both preflight and on-orbit conditions. Thus, this theoretical prediction agrees with the calculations given here. We conclude that dark current is a minor source of radiometric error, even for dark targets.

### 3.3 Signal chain: Square-root encoding

MISR makes use of square-root data encoding in order to decrease the data rate required from the spacecraft to the ground station. The algorithm to encode MISR digital numbers (DN) into a compressed number is as follows:

$$DN_{\text{encoded}} = \text{round}(32.0 * \sqrt{\text{float}(DN)}) \quad (3)$$

During data processing these numbers are restored to their linear representation. To decode these numbers, the following operation is performed:

$$DN_{L1A} = \text{round}(\text{float}(DN_{\text{encoded}})/32.0)^2 \quad (4)$$

here  $DN_{L1A}$  are DN numbers that are reported to the Level 1A data product. They are only approximately equal to the original camera DN output, because the compression scheme cannot be perfectly reversed.

One can now estimate the percentage radiometric error, by assuming a typical overclock value:

$$DN_{\text{overclock}} = 350 \quad (5)$$

$$\% \text{ error} = (DN_{L1A} - DN) * 100 / (DN - DN_o) \quad (6)$$

It is thus shown that the radiometric error attributable to square-root encoding is 0.5% for DN greater than 200 DN above overlock (an equivalent reflectance of 0.005), and decreases with increasing illumination. The error due to square-root-encoding is therefore considered negligible.

### 3.4 Optical effects: Ghosting

Figure 4 shows an iceberg surrounded by a dark ocean. The image was acquired on December 9, 2001, over the Ross Sea. The lower image shows a highly contrast-stretched image of the normal view, shown above. The iceberg shown in the lower figure is an inverted, blurred ghost image of the original iceberg. The reflectance of the ice is approximately 0.4, all bands, whereas the ocean reflectance varies from 0.06 to 0.01 in going from the Blue to NIR wavelengths. In this image 0.3% of the bright target has been reflected into the adjacent dark ocean. For ghosting of this magnitude, a target brighter than  $\rho_{toa}=0.66$  would be required in order to induce a radiometric error of 10% in a dark ocean scene of magnitude 0.02. The dark target would have to be located specifically in the ghost location. We conclude that for all but a small number of cases, ghosting will not impact radiometry over dark ocean targets.

sult in a shadow where the image had been. We also know that only the A and D cameras were tuned to produce blurred ghost images. This was never done for the B and C cameras. The degree of focus for these ghost images, therefore, is unknown and camera dependent.

### 3.5 Optical effects: Point-spread-function response

The image of a point object source is always blurred due to diffraction, lens aberrations, and scattering. This output response to a point source is known as the point-spread-function (PSF) for a given optical system. MISR PSF functions have been measured pre-flight.

For an in-flight determination of the PSF, the derivative of the edge response was taken using the iceberg edge of the December 9, 2001 Antarctica scene. The updated response was found to have the same shape, but with a larger halo, as compared to the preflight measurement. These preflight and in-flight derived PSF kernels are shown in Figure 5. This figure indicates that the preflight PSF's underestimate the amount of contrast adjustment needed.

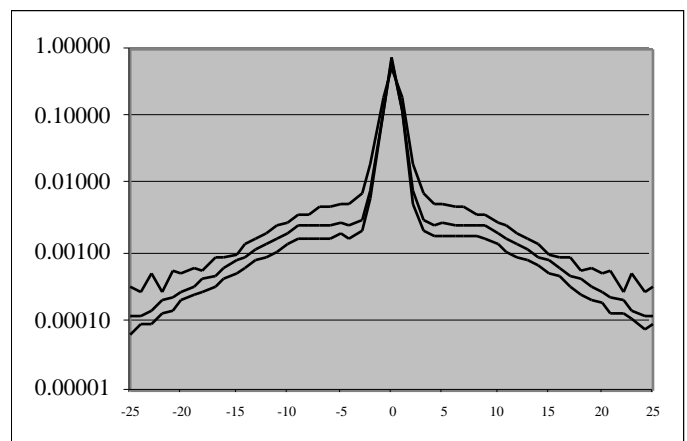


Figure 5. Comparison of preflight and in-flight empirical PSF's. Curves from top to bottom are in-flight derived, operational functions, and preflight measurements.

Figure 4. Ghosting in the MISR Bf-NIR band. Data were acquired over the Ross Sea, Orbit 10521, Path 54. The ice TOA reflectance is on the order of 0.43, with a dark ocean of 0.06 - 0.01 for the Blue to NIR bands.

No attempt is made to correct for the ghosting, as the effect is small, and as the secondary image is not in focus. Any attempt to remove the ghost would re-

PSF correction is done on all MISR radiance data products. The operational PSF functions were derived by the following procedure:

- 1) Start with the preflight point spread function
- 2) Average right and left about the center to make it symmetric.
- 3) Multiply the entire function by a scale factor that adjusts the background halo to that empirically derived from the on-orbit data. A value of 1.5 has been used to produce the operational kernels.
- 4) Renormalize to unit area by adjusting the energy in the central 3 pixels (which contain ~95% of the energy)
- 5) Take the inverse Fourier transform (FT).

6) Multiply the inverse Fourier transform by the Fourier transform of the central 9 pixels of the PSF (the “core”). This step is performed so that the deconvolved images correspond to the PSF of the core, rather than a delta function, and is done to avoid ringing at contrast boundaries.

7) Inverse transform, take the real part, and average left/right to correct any numerically-induced asymmetries.

It is believed that this procedure minimizes the ringing associated with a sharper PSF core, and improves the contrast. Inspection of MISR Level 1B2 radiance products reveal that sharp radiance discontinuities can be observed in the presence of contrast edges, such as iceberg edges. This is validation of the PSF deconvolution process.

## 4 CROSS-COMPARISON STUDIES

### 4.1 MODIS

MODIS is an useful sensor with which to cross-compare radiometric products. The MODIS pass-band parameters, when derived using the MISR moments analysis algorithm, are listed in Table 3. MODIS Band 4 (land) and Band 9 (ocean) are examples of bands that are well matched for the two sensors. For all bands a radiometric correction is made to predict the radiance that MODIS would have reported, had it been built with MISR bandpasses. This spectral-correction algorithm has been described in Bruegge et al. (2002). MISR to MODIS radiance ratios reported in this Section have all had these spectral corrections performed.

[Table 3 is at the end of the document]

Table 3. MODIS spectral parameters. The last two columns give spectral correction factors for two scene types.

MODIS reports a reflective solar bands (RSB) calibration uncertainty of 2% for the reflectance factor and 5% for the radiance product. Both land and ocean channel calibrations utilize a solar diffuser (SD). In addition to a direct view of the panel, a second data set is acquired using a 7.8% transmission screen deployed in front of the SD. This calibrates those channels that would otherwise saturate.

The MODIS detectors view the calibrated SD to place their data products on a TOA reflectance scale. The measurement precision is about 0.2 to 0.5% depending on the bands or if the SD screen is used in the calibration (ocean bands use the SD screen for the calibration). SWIR band uncertainties are higher due to residual crosstalk errors.

The solar diffuser stability monitor (SDSM) is used to track SD degradation. The SDSM is a small

integrating sphere and filtered detectors that look at the sun and SD respectively. The ratio of the SD to the sun view provides a measure of the spectral reflectance of the SD, thus tracks the SD degradation. The SDSM makes use of a 2% transmission screen when viewing the Sun. This is done to place the incoming signal on the same point on its dynamic range curve.

More recent data use a direct view of the SD for both the land and ocean channels. The MODIS calibration team has found that the difference in using the screen or not using the screen is less than 1%. Thus they believe the relative calibration between the ocean and land bands is within 1%.

Figure 6 compares the radiances measured by several sensors against the vicarious calibration radiances conducted July 22, 2003. For comparisons over uniform desert playa, MISR is typically 3-7% brighter than MODIS, for MISR data of "linear-offaxis" heritage. The agreement is within 4% for MISR "band-adjusted" version data. The radiometric bias between MISR and MODIS can be traced to the utilization of different standards and processes used to establish their respective scales. (Kurt Thome, University of Arizona, provides VC datasets for the MODIS team, and reports a discrepancy of -1.4, -0.9, -3.4, -2.5, and -3.4% respectively, for the MODIS 412, 469, 555, 645, 858 nm bands. MODIS radiances are lower than his VC observations. As MISR is calibrated against a VC standard, greater consistency between MISR and a VC-adjusted MODIS is found.) MODIS VC studies are done using the land channels, as the ocean channels saturate over these bright targets.

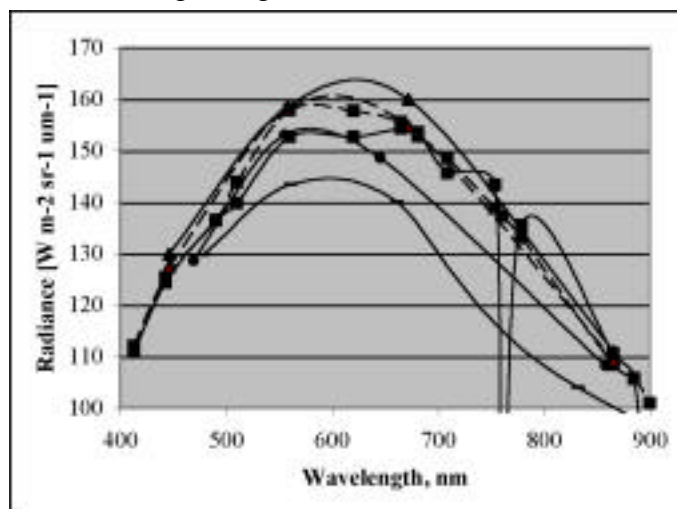


Figure 6. Measured radiances from Vicarious Calibration data, MISR, MERIS, MODIS, and Landsat. Data were acquired July 22, 2003 at Railroad Valley, Nevada.

MISR and MODIS comparisons were next made over uniform dark oceans. One such example is provided in Figures 7-9. In Figure 7 an area of the Arabian Sea is shown. Taking radiances from a clear, dark ocean target, the equivalent reflectances from

MISR and MODIS are shown in Figure 8. In making a large number of such comparisons, we generally see that MISR data agree with MODIS land-channel data, to within 3%, when land targets are observed. For ocean targets, the agreement between MISR and MODIS ocean-channel data is comparable.



Figure 7. MISR image, Arabian Sea, 06-April-2001.

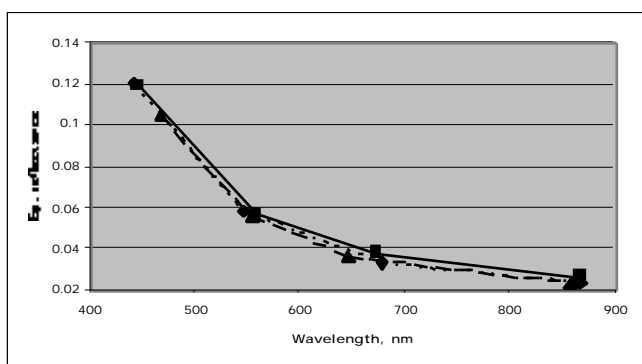


Figure 8. A comparison of radiometry from MISR (squares), MODIS land channels (long dash, triangles), and MODIS ocean channels (dash, diamonds), for a dark ocean target. Data are for the above dark ocean target, 57.43° E, 17.80° N.

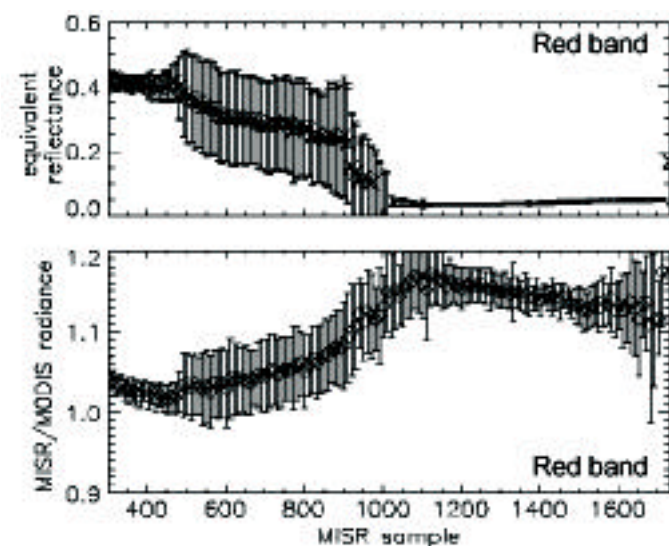


Figure 8. Top) Plot of mean equivalent reflectance versus sample, for the Arabian Sea image shown above. The mean is calculated by averaging MISR or MODIS radiances in the vertical (north-south) direction. Standard deviations around the mean are also shown. High standard deviations are where both land and water figure into the calculations. Bottom) Median MISR/MODIS radiance ratio at each sample location, calculated by combining all points in the north-south direction. Standard deviations are also shown. Note the inconsistency between the ratio over water (dark scene) relative to land (bright scene).

Figure 9 shows a discrepancy between MISR and MODIS-land channels, when an ocean scene is observed. In this figure the scene is half land and half ocean. The upper figure shows the column averages and standard deviations of radiances, for both MISR and MODIS. The lower image shows the median ratio. It is noted that the ratio agrees well over land, but increases over ocean. This suggests a non-linearity in one or the other sensor. It is noted that MISR is an all-refractive system, with a Lyot depolarizer as its front element. MISR is insensitive to polarization effects. Since MODIS may have greater polarization sensitivity, this may partially explain the variation in the ratio for the ocean site, as compared to the land. A more detailed validation of MODIS radiometry, using the ocean bands, is ongoing by the MODIS ocean community. Further validation studies on the radiometric response of MODIS land channels, over dark ocean targets, are needed. (It is noted that MODIS land channels are used to retrieve aerosol properties over ocean sites.) Issues that the MODIS team are investigating include uncertainties in the SD reflected light due to excess radiance (scattering or Earthshine), uncertainties in the effects of the SD attenuation screen, and changing polarization sensitivity.

To summarize, MISR and MODIS radiance data agree to within a 4% uncertainty, providing that the MODIS land channels are used over land and the MODIS ocean channels are used over ocean. The agreement of the ocean values, using the MODIS ocean channels, provides a validation of MISR radiometry at these low-light levels.

#### 4.2 Lunar observations

Lunar observations are routinely used by SeaWiFS (Barnes et al. 1999), an ocean viewing sensor, to track degradation with time. On April 14, 2003, MISR had its first opportunity to view the Moon. A special maneuver of the Terra spacecraft was performed, on this date, as it traversed the nightside of the orbit. The maneuver entailed a backwards somersault of the spacecraft as it pitched end-over-end, allowing the normally Earth-viewing instruments to look at deep space and the waxing Moon. The purpose of this acrobatic feat was to assist in the cross-comparison of MISR, MODIS, and ASTER (all Terra instruments) as well several other sensors on an assortment of platforms. During a 16-minute interval, the lunar disk passed through the fields-of-view of all nine MISR cameras, resulting in a unique set of images. Figure 10a shows one such image, for the high-resolution Df-Red channel. Familiar lunar features are clearly recognizable. The dark lunar "maria" are vast plains of basaltic lava.

Lunar data were acquired in Global Mode, with 12 high-resolution channels (Fig. 10a) and 24 channels in 4 pixel by 4 line averaging mode, called 4x4

(Fig. 10b). Varying resolution is also encountered with the four camera designs, due to differences in focal lengths. Examples of the resolution with camera design are shown in Figure 11.

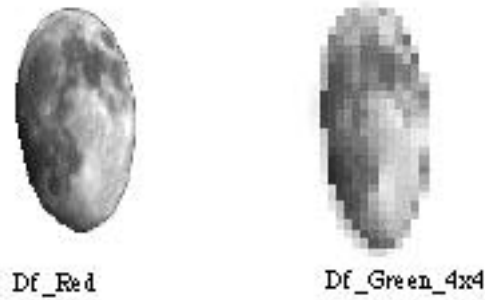


Figure 10. MISR viewed the moon in its baseline Global Mode configuration. (a) Twelve of the 36 MISR channels are configured to high-resolution (no averaging) during Global Mode, including this Df\_Red image. (b) Twenty-four channels are in 4x4 pixel averaging mode, such as this Df\_Green\_4x4 image.

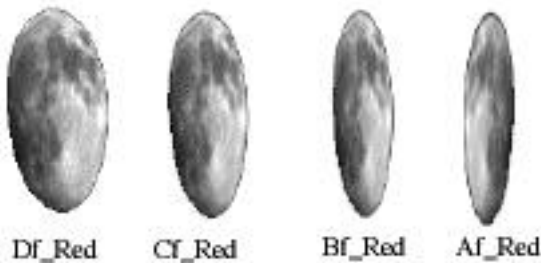


Figure 11. Lunar image resolution degrades in going from the D to A camera design, due to the smaller focal lengths in going from D to A.

These data were then used to derive a measure of the lunar irradiance, which was compared to that of the empirically derived Robotic Lunar Observatory (ROLO) model. In computing this irradiance, we must account for a large amount of oversampling. The equation used for this analysis sums the radiance samples, multiplies by the detector solid angle, and corrects for oversampling.

$$\begin{aligned} \text{Lunar Irradiance [mW m}^{-2} \text{ nm}^{-1}] = & \\ & (\text{fraction of IFOV not in previous samples}) * \\ & (\text{detector solid angle [sr]}) * \\ & (L \text{ [mW m}^{-2} \text{ sr}^{-1} \text{ nm}^{-1}]) \end{aligned}$$

The required inputs are given in Table 4.

Table 4. Lunar calibration parameters for April 14, 2003

---

Lunar observation date: April 14, 2003
Orbit: 17672
Time: 2200-2220 UT
Planned Terra pitch rate: D [rad/ sec]= 0.002129, or 0.122 deg/ sec
Lunar distance: D [1000 km] = 366.5-6371/ 1000-1738/1000-0.705=357.7
MISR camera sampling rate: tsamp [msec] = 40.8

---

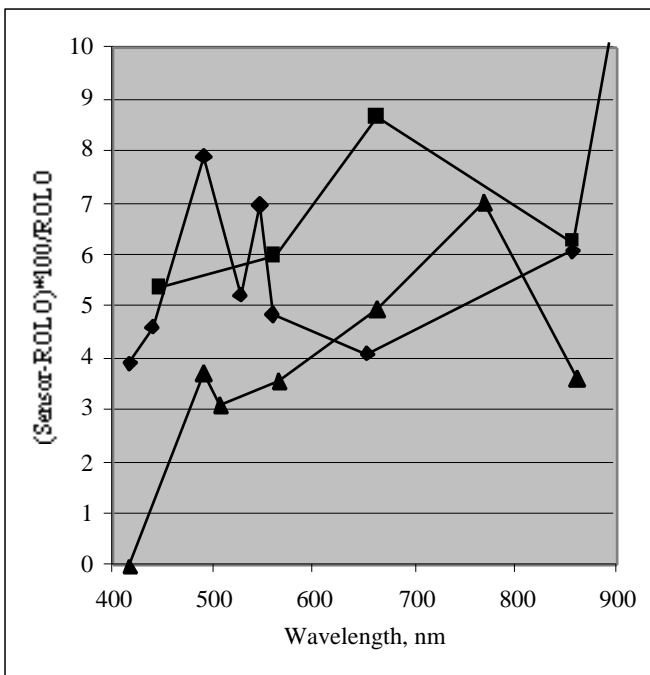
Camera focal length, Df-Da order: f [mm]={123.67, 95.34, 73.02, 58.90, 58.90, 59.03, 73.00, 95.32, 123.65}  
 Crosstrack detector dimension: Dxdet [mm] = 21  
 Alongtrack detector dimension: Dydet [mm] = 18  
 Sum of MISR radiance samples: L [mW m<sup>-2</sup> sr<sup>-1</sup> nm<sup>-1</sup>]  
 fraction of IFOV not in previous sample: tsamp\*D\*f/Dxdet  
 detector solid angle [sr]: Dxdet\* Dydet\* 10<sup>-6</sup> / f<sup>2</sup>

---

The results of this comparison are shown in Figure 12. Although there appears to be a 5% bias between MISR and ROLO, in fact a similar bias is found between the ROLO model and SeaWiFS, as well as between the model and MODIS land channels (Kieffer 2003). It is concluded that the lunar observations confirm that MISR radiometry is consistent with MODIS land channels, as well as SeaWiFS, for this low-light, small extent target.

The accuracy of the MISR measure of lunar irradiance is limited by the oversampling correction. Its uncertainty is at least 5%, based upon the scatter of measurements from the nine MISR cameras. Nevertheless, the experiment proved to be extremely valuable for the MISR community, in that it validated the band-adjustment values obtained from the vicarious calibration experiments (Fig. 2), as well as confirmed that the absolute radiometry is consistent with comparisons made over land targets. Our confidence in MISR radiometry over low-level targets is therefore increased due to this experiment.

Figure 12. Differences between MISR (squares), MODIS (dia-



monds), and SeaWiFS (triangles), as compared to the ROLO measure of lunar irradiance.

## 5 CONCLUSIONS

The MISR calibration and science teams have carefully reviewed the contributors to radiometric accuracy over low-light scenes. As with any instrument, radiometry for these conditions is challenging. We have investigated the impact of electronic bias, dark current, and data compression, and find no evidence that these error sources are degrading the quality of the data. It is felt, however, that system-level validation offer the best evidence of radiometric accuracy. Cross-comparison with MODIS over both ocean and lunar observations demonstrate the consistency of data for dark targets, as do dark-water vicarious calibrations. For these reasons we conclude that MISR is meeting its absolute calibration specification for dark water conditions, including an uncertainty specification of 10% at  $\rho_{\text{toa}}=0.02$ . Further, for data processed after November 2003, we conclude that the band-relative requirement for an uncertainty of 1% is also being met throughout the dynamic range of the instrument.

This experience has led us to propose, for future missions, that:

- a floating electronic bias should NOT be added to a signal chain;
- Spectralon does not degrade on-orbit, if contamination is avoided;
- multiple methodologies are required in any calibration program as not all pathways will succeed;
- cross-comparisons of sensors need to be made at a range of illumination levels, crosstrack view angles, and scene contrasts; and

- establishing a calibration over desert targets is only the first step in achieving a calibrated instrument. Science communities need to make use of a range of scene brightness and contrast conditions in their validation studies.

## 6 ACKNOWLEDGMENTS

The work described in this paper has been carried out at the Jet Propulsion Laboratory, California Institute of Technology, under contract with the National Aeronautics and Space Administration. MISR data products are processed and made available by the Atmospheric Sciences Data Center, Langley Research Center.

A number of support individuals have assisted in the acquisition and analysis of MISR calibration data, including Nadine Chrien, Mike Smyth, David Nelson, Kyle Miller, Tom Thaller, and Tom Nolan. The authors also wish to thank the following individuals who have participated in Peer Reviews of MISR calibration: Roger Davies, Michael Gunson and Cinzia Zuffada, JPL; Brian Markham, Landsat Calibration, GSFC; Stu Biggar, Vicarious calibration, Univ. of Arizona; James Butler, EOS Calibration Scientist, GSFC; Bruce Guenther, MODIS Calibration, GSFC; and Jeff Mendenhall, ALI Design Engineer, Lincoln Labs.

Finally, Jack Xiong, GSFC, and Kurtis Thome are to be thanked for many useful discussions and data exchanges.

## REFERENCES

- Abdou, Wedad A., Mark C. Helmlinger, James E. Conel, Stu Pilorz, Carol J. Bruegge, Barbara J. Gaitley, and John V. Martonchik, 2000. Ground measurements of surface bidirectional reflectance factor (BRF) and hemispherical directional reflectance factor (HDRF) using the portable Apparatus for Rapid Acquisition of Bidirectional observation of the land and atmosphere (PARABOLA III), *J. Geophys. Res.*, 106:11,967 - 11,976.
- Abdou, W., C. Bruegge, M. Helmlinger, J. Conel, S. Pilorz, & B. Gaitley 2002. Vicarious calibration experiment in support of the Multi-angle Imaging SpectroRadiometer (MISR), *IEEE Trans. Geosci. Remote Sens.*, 40(7):1500-1511.
- Barnes, Robert A., Robert E. Eplee, Jr., Frederick S. Patt, & Charles R. McClain 1999. *Applied Optics*, 38(21):4649-4664.
- Bruegge, Carol J., Nadine L. Chrien, Robert R. Ando, David J. Diner, Wedad A. Abdou, Mark C. Helmlinger, Stuart H. Pilorz, & Kurtis J. Thome, 2002. Early Validation of the Multi-angle Imaging SpectroRadiometer (MISR) Radiometric Scale, *IEEE Trans. Geosci. Remote Sens.*, 40(7):1477-1492.
- Bruegge, Carol, Nadine Chrien, & David Haner, 2001. A Spectralon BRF data base for MISR calibration applications *Remote Sensing of Environment*, 76: 354-366.

Bruegge, C., V. Duval, N. Chrien, & D. Diner 1993a. Calibration Plans for the Multi-angle Imaging SpectroRadiometer (MISR), *Metrologia*, 30(4):213-221.

Bruegge, Carol J., Mark C. Helmlinger, James E. Conel, Barbara J. Gaitley, & Wedad A Abdou, 2000. PARABOLA III: a sphere-scanning radiometer for field determination of surface anisotropic reflectance functions, *Remote Sensing Reviews*, 19:75-94.

Bruegge, C., A. Stiegman, R. Rainen, A. Springsteen, 1993b. Use of Spectralon as a diffuse reflectance standard for in-flight calibration of earth-orbiting sensors, *Opt. Eng.*, 32(4):805-814.

Chrien, N., C. Bruegge, & R. Ando, 2002. Multi-angle Imaging SpectroRadiometer (MISR) on-board calibrator (OBC) in-flight performance studies, *IEEE Trans. Geosci. Remote Sens.*, 40(7): 1493-1499 .

Diner, D.J., L.M. Barge, C.J. Bruegge, T.G. Chrien, J.E. Conel, M.L. Eastwood, J.D. Garcia, M.A. Hernandez, C.G. Kurzweil, W.C. Ledebauer, N.D. Pignatano, C.M. Sarture, and B.G. Smith, 1998a. The Airborne Multi-angle SpectroRadiometer (AirMISR): instrument description and first results, *IEEE Trans. Geosci. Rem. Sens.*, 36:1339-1349.

Diner, D.J., Beckert, J.C., Bothwell, G.W. and Rodriguez, J.I., 2002. Performance of the MISR Instrument During Its First 20 Months in Earth Orbit, *IEEE Trans. Geosci. Remote Sensing*, 40(7):1449-1466.

Diner, D., J. Beckert, T. Reilly, C. Bruegge, J. Conel, R. Kahn, J. Martonchik, T. Ackerman, R. Davies, S. Gerstl, H. Gordon, J-P. Muller, R. Myneni, R. Sellers, B. Pinty, & M. Verstraete 1998b. Multi-angle Imaging SpectroRadiometer (MISR) description and experiment overview, *IEEE Trans. Geosci. Rem. Sens.*, 36:1072-1087.

Early, E.A., P.Y. Barnes, B.C. Johnson, J.J. Butler, C.J. Bruegge, S.F. Biggar, P.R. Spyak, M.M. Pavlov, 2000. Bidirectional reflectance round-robin in support of the Earth Observing System program, *American Meteorological Society*, August:1077-1091.

Kahn, R., W-H. Li, C. Bruegge, J. Martonchik, D. Diner, B. Gaitley, O. Dubovik, B. Holben, A. Smirnov, Z. Jin, and D. Clark, 2004. MISR low-light-level calibration, and implications for aerosol retrieval over dark water, *J. Geophys. Res.*, submitted for publication.

Kahn, Ralph, Pranab Banerjee, & Duncan McDonald, 2001. The sensitivity of multi-angle imaging to natural mixtures of aerosols over ocean, *J. Geophys. Res.*, 103(D24): 32195-32213.

Kahn, Ralph, Pranab Banerjee, Duncan McDonald, & David J. Diner, 1998. Sensitivity of multiangle imaging to aerosol optical depth and to pure-particle size distribution and composition over ocean, *J. Geophys. Res.*, 103(D24):32,195-32,213.

Kieffer, Hugh, 2003. Conference proceedings, Characterization and radiometric calibration for Remote Sensing, Logan, Utah, September 15-18.

Marchand, Roger, 2004. Publication in preparation.

Stiegman, A.E., C.J. Bruegge, A.W. Springsteen, 1993. Ultraviolet stability and contamination analysis of Spectralon diffuse reflectance material, *Opt. Eng.* 32(4):799-804.

World Climate Research Programme (WCRP) Publication Series No. 7, WMO ITD-No. 149:119-126, October 1986. The data was compiled by Christoph Wehrli, World Radiation Center (NRC), Davos-Dorf, Switzerland under WRC Publication No. 615, July 1985.

MISR Band no.	Sensor	$\lambda_c$ , nm	$\delta\lambda$ , nm	$E_{0,b}$ $Wm^{-2}\mu m^{-1}$	Sens radiε factc
					Desc
1	MODIS Band 3	466	21	2015	0.90
2	MODIS Band 4	554	21	1858	1.00
3	MODIS Band 1	646	50	1601	0.98
4	MODIS Band 2	856	45	989.8	0.98
1	MODIS Band 9	442	11	1865	1.01
2	MODIS Band 12	547	12	1870	1.01
3	MODIS Band 14	677	14	1505	1.00
4	MODIS Band 16	866	19	969.7	1.00

Table 3. MODIS spectral parameters. The last two columns give spectral correction factors for two scene types.